Enhanced finite size and interface mixing effects in iridium manganese ultra thin films

Sarah Jenkins, and Richard F. L. Evans

Enhanced finite size and interface mixing effects in iridium manganese ultra thin films

Sarah Jenkins[a] and Richard F. L. Evans[b]
Department of Physics, The University of York, York YO10 5DD, United Kingdom

The finite size and temperature dependent properties of antiferromagnets are of critical importance to a wide range of spintronic and neuromorphic computing devices. Here we present atomistic simulations of IrMn, one of the most technologically important antiferromagnets, in both the ordered ($L1_2$) and disordered (γ) phases. We have found that antiferromagnetic $IrMn_3$ films show a stronger finite size dependence of the Néel temperature than an equivalent ferromagnet due to the existence of spin frustration. We also find that the disordered γ-$IrMn_3$ phase shows a dramatic reduction in the Néel temperature to less than room temperature for films less than 1 nm thick. Interfacial intermixing of the $IrMn_3$ with a non-magnetic Cu capping layer further reduces the Néel temperature for a given film thickness, with a stronger influence on the disordered γ-$IrMn_3$ phase compared to the ordered $L1_2$-$IrMn_3$ phase. Our results suggest a larger antiferromagnetic film thickness is required for devices operating at or above room temperature compared to an equivalent ferromagnet, particularly for sputtered films with a high degree of interfacial intermixing. *Published by AIP Publishing.*
https://doi.org/10.1063/1.5038006

I. INTRODUCTION

Antiferromagnetic spintronics[1,2] is a newly emerging field which has renewed interest in antiferromagnetic (AFM) materials. Antiferromagnets were once thought to be of limited practical use due to their weak interaction with external magnetic fields,[3] but when coupled to a ferromagnet to induce exchange bias, they find extensive applications in magnetic recording and thermally assisted magnetoresistive random access memory.[4,5] More recently, the discovery of electrical switching of antiferromagnets by staggered spin-orbit torque[6,7] has led to renewed interest in the fundamental properties of antiferromagnets for spintronics. Antiferromagnets also exhibit ultrafast inertial dynamics due to the balanced nature of magnetic moments at the atomic level which may lead to further improvements in energy efficiency and speed compared to conventional ferromagnetic devices.

Neuromorphic computing[8] is an emerging field which aims to replicate the cognitive capabilities of biological systems and apply them to complex computing problems such as pattern recognition, to study the large scale behavior of cognitive systems and explore new concepts in artificial intelligence. Magnetic devices offer significant potential as artificial neurons due to their intrinsic hysteretic properties[9] and ability to retain their state for extended periods of time. Combining the low power processing capabilities and fast dynamics of antiferromagnetic spintronic devices could enable ultra-low power neuromorphic computing devices. Recently, Fukami *et al.*[10] developed such a device utilizing exchange bias to preserve its output state while using spin-orbit torque for electrical switching. Once developed,

this will allow for devices which can complete complex tasks at high speeds with a low power consumption that can outperform conventional von Neumann computers.[8,11] Practical spintronic devices rely on interfacial magnetic effects at the atomic scale and so the antiferromagnetic layers have a typical thickness of only a few nanometers. Understanding these effects is particularly important for spin-orbit torque driven devices which rely on interfacial properties for thermal stability and generating torques. Finite size effects in ferromagnets are well understood, but are little studied in antiferromagnets, particularly in materials of practical importance such as iridium manganese (IrMn) alloys.[12] IrMn is particularly important due to its high thermal stability[13,14] and high magnetocrystalline anisotropy energy density[15,16] and exhibits the largest exchange bias of any known antiferromagnet. Exchange bias provides a unidirectional anisotropy when coupling a ferromagnet (FM) to an antiferromagnet (AFM), causing the FM to be pinned along one direction. The pinning is useful in memory storage and is utilised in many devices such as read heads, spin valves, and magnetic sensors. In these devices, the AFM plays a supporting role, but their finite size effects are complex. Previously, Frangou *et al.* found that for films less than 3 nm thick, there was a linear decrease of the Néel temperature and for 0.5 nm films, the Néel temperature falls to only 50 K. They note the agreement with the work of Petti *et al.*[17] who used nanocalorimetry to calculate the Néel temperature of 2 nm thin films of IrMn. The Néel temperature of the 2 nm thick film had reduced to 173 K, about 20% of the bulk value they calculated. The finite size properties are dependent on the film thickness and ordering and still subject to some interpretation.

Here we present atomistic simulations of the effects of film thickness and interfacial intermixing on the temperature dependent properties of $IrMn_3$ alloys. We consider both $L1_2$ ordered and disordered (γ) phases of $IrMn_3$, which have

[a] sarah.jenkins@york.ac.uk
[b] richard.evans@york.ac.uk

different ordering temperatures and thermal stabilities. We have found that there is a weak thickness dependence of the Néel temperature for films thicker than 2 nm, while for ultra thin films of a few atomic layers, we find a catastrophic collapse in the Néel temperature to a few Kelvin. We find that interface mixing is in general a weak effect except at the smallest thickness's where the existence of point defects at the surface leads to large fluctuations of surface spins and a stronger reduction in the Néel temperature for a given film thickness.

II. ATOMISTIC SPIN MODEL

To model the magnetic properties of the antiferromagnet (AFM) IrMn, we have developed an atomistic spin model with Heisenberg exchange.[18] IrMn alloys have a base face-centred cubic (FCC) unit cell where each of the four sites in the unit cell is magnetically distinct, each comprising a different magnetic sublattice. Here, we focus on the technologically relevant $IrMn_3$ composition considering the ordered $L1_2$-$IrMn_3$ and γ-$IrMn_3$ phases. In general, it is expected that sputtered devices have a relatively low order parameter due to the difficulty in achieving ordered $IrMn_3$ and so have properties closer to the γ-$IrMn_3$ phase. In the fully disordered (γ) phase, the Ir atoms are randomly distributed in the four crystal sites within the full crystal lattice. In the fully ordered ($L1_2$) phase, the Ir atoms are all positioned in the same magnetic sublattice. The model assumes a localized spin density at the Mn atomic sites which forms a fixed length classical spin magnetic moment $\mu_s = 2.65\mu_B$ calculated from first principles simulations.[16] The Ir sites are treated as nonmagnetic impurities that induce a strong spin-orbit coupling effect in the Mn sites. The energy of the system is defined using a spin Hamiltonian of the form:

$$H = -\sum_{i<j} J_{ij}\mathbf{S}_i \cdot \mathbf{S}_j - \frac{k_N}{2}\sum_{i \neq j}^{z}(\mathbf{S}_i \cdot \mathbf{e}_{ij})^2, \qquad (1)$$

where i, j represent local and neighboring atomic sites and $\mathbf{S}_i$ and $\mathbf{S}_j$ the respective spin directions. The effective exchange interactions J_{ij} were limited to nearest antiferromagnetic ($J_{ij}^{nn} = -6.4 \times 10^{-21}$) and ferromagnetic next nearest ($J_{ij}^{nnn} = 5.1 \times 10^{-21}$) neighbors and assumed to be
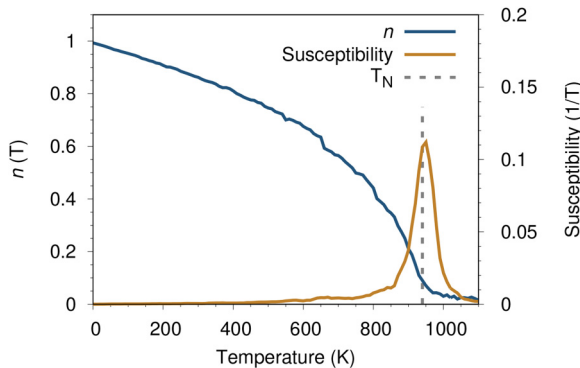
independent of the local atomic ordering. This is justified from first principles simulations which show a similar interatomic range dependence of exchange interactions for the ordered $L1_0$ and $L1_2$ phases of IrMn.[16] The magnetocrystalline anisotropy in $IrMn_3$ is assumed to arise from the large spin-orbit coupling between Mn and Ir sites. Usually, the magnetocrystalline anisotropy energy must be determined from first principles *ab initio* calculations.[16] First principle calculations are particularly challenging for disordered alloys, where the large number of local atomic environments around the Mn sites due to the random placement of Ir in the crystal. We therefore use an approximate yet robust approach using the Néel pair anisotropy model,[3,19] where $\mathbf{S}_i$ and $\mathbf{S}_j$ are unit vectors describing the spin direction at the local site i and neighboring j sites, respectively. $k_{ij} = 4.22 \times 10^{-22}$ is the Néel pair anisotropy constant between Mn and Ir sites and $\mathbf{e}_{ij}$ is a unit position vector between nearest neighboring Mn and Ir sites.

The temperature dependent properties of the system are simulated using a metropolis Monte Carlo algorithm, the Hinzke-Nowak update algorithm,[20] and a combination of spin-flip, random, and Gaussian trial spin moves. Each sample was initially equilibrated at a temperature of 1500 K (above the Néel temperature) to thermalize the spins. The system was then cooled to 0 K using a linear cooling function over 1 000 000 Monte Carlo steps to find a ground state spin configuration. The system was then heated back up to 1500 K to find the Néel temperature in steps of 10 K performing 10 000 equilibrating Monte Carlo steps and then averaging over a further 10 000 Monte Carlo steps. All numerical simulations were performed using the VAMPIRE software package.[18,21]

The Néel temperature is determined from the mean sublattice magnetization n, which is the average magnetization length calculated from a summation over the spins of each distinct magnetic sublattice. As a classical simulation, the temperature dependent magnetization is accurately described by the fitting function

$$n(T) = n_0\left(1 - \frac{T}{T_N}\right)^{\beta}, \qquad (2)$$

where n is the average sublattice magnetization, n_0 is the average zero-temperature ordering of the sublattices, T is the temperature, T_N is the Neel temperature, and β is the critical magnetization exponent. It is possible to calculate the Néel temperature from the sublattice magnetization against temperature curve. However, for small sizes, the fitting becomes inaccurate due to a reduced criticality of the magnetization, and so we extract the Néel temperature from the peak in the isotropic longitudinal susceptibility χ_n for each sublattice given by

$$\chi_n = \frac{\sum_i \mu_i}{k_B T}\left(\langle|n|^2\rangle - \langle|n|\rangle^2\right), \qquad (3)$$

where i are indices of atoms within the same sublattice. Figure 1 shows a typical simulation result for a $(10\,\text{nm})^3$ cube of $L1_2$ $IrMn_3$ showing the usual decrease in sublattice spin order with increasing temperature due to spin fluctuations. The sublattice susceptibility diverges at the Néel temperature with a well defined peak from which we extract the T_N.

FIG. 1. Plot of the average sublattice magnetization n and isotropic longitudinal susceptibility χ_n as a function of temperature for the $L1_2$ phase of $IrMn_3$. The Néel temperature T_N is extracted from the peak in the susceptibility and is close to the bulk value[14] of 1000 K.

III. BULK MAGNETIC PROPERTIES OF IRIDIUM MANGANESE

To validate our model, we have simulated the ground state spin structures of the ordered L1$_2$ and disordered γ phases of IrMn$_3$ as shown in Fig. 2 using the Monte Carlo Metropolis algorithm by zero-field cooling from above the Néel temperature to 0 K. In agreement with previous experimental[13,14] and *ab initio* results,[16] we find ordered L1$_2$-IrMn$_3$ has a triangular (T1) spin structure where the magnetic moments lie in plane along the [111] planes with an angle of 120° between them pointing along the [211] directions and that disordered γ-IrMn$_3$ has a tetrahedral (Q3) spin structure[13] where the magnetic moments point 109.5° apart.

Our simulations reproduce the different ordering temperatures of the L1$_2$ ($T_N \sim 1000$ K) and γ ($T_N \sim 700$ K) despite using the same Spin Hamiltonian and both ordered $L1_2$-IrMn$_3$ and disordered γ-IrMn$_3$ having the same average number of exchange bonds. This arises due to different degrees of geometric frustration in the spin structures. All Mn spins in the system energetically prefer full antiferromagnetic alignment (180°), but due to the geometric arrangement and high coordination numbers, this spin structure is not possible. Therefore, in the ground state, the spins are already frustrated and so thermal spin fluctuations have a stronger effect on the sublattice ordering in the γ phase compared to the L1$_2$ phase. This naturally leads to a lower ordering temperature in the γ-IrMn$_3$ phase.

IV. FINITE SIZE EFFECTS IN ULTRATHIN IrMn FILMS

The properties of ultrathin films of IrMn$_3$ were modeled assuming the layer is sandwiched between non-magnetic Cu layers with low spin-orbit coupling so that they have no influence on the magnetic parameters other than the loss of Mn exchange bonds at the surface of the film. The simulated system has fixed lateral dimensions of 15 nm × 15 nm with periodic boundary conditions in the plane and a varying thickness in the range 0.25–10 nm. A visualization of the generated crystal structure for the disordered γ phase is shown in Fig. 3. Initially, the interface between the Cu and
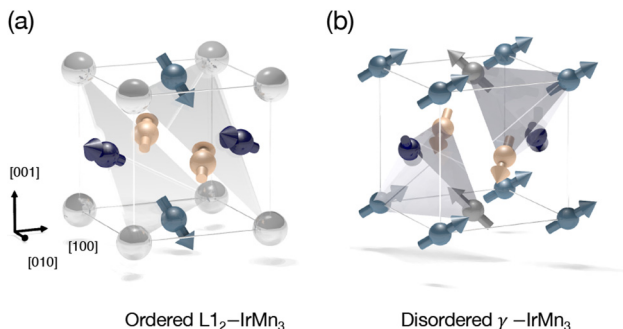

FIG. 2. Visualization of the simulated ground state spin structures of IrMn$_3$ obtained from zero-field cooling. The spins show an average spin of each magnetic sublattice direction over the whole sample. In the case of L1$_2$-IrMn$_3$, the corner atoms are all Ir and so have no net magnetic moment. The spin structures are in excellent agreement with experimental measurements and first principles simulations.
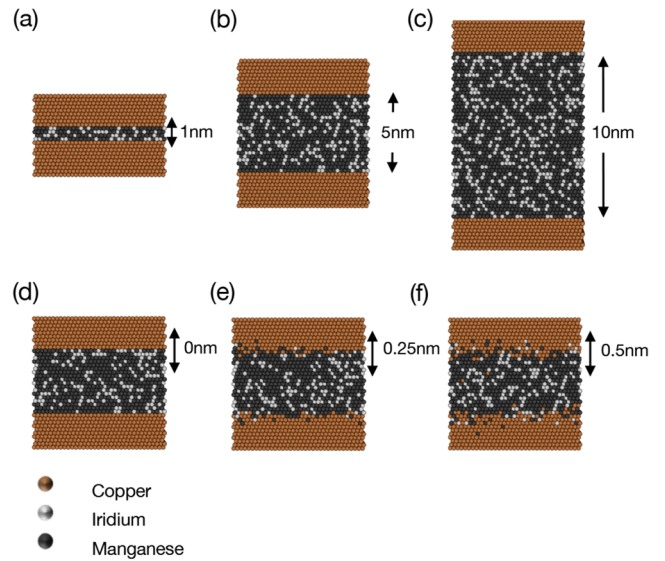

FIG. 3. Atomistic visualization of the generated thin film system for the $\gamma IrMn_3$ phase for different film thicknesses (a) 1 nm, (b) 4 nm, and (c) 10 nm. The colors represent different atomic species. The same is shown for different levels of interface mixing with interface widths of (d) 0 nm, (e) 0.25 nm, and (f) 0.5 nm.

IrMn$_3$ is assumed to be atomically flat, but we also study the case of intermixing between the layers to recreate the effects of sputtered films where atomic mixing is more likely to occur. The mixed interface was generated using a probability distribution defined by

$$P(z) = 1 - \frac{1}{2}\tanh\left[\frac{\pi(z - z_0)}{w}\right],\tag{4}$$

where $P(z)$ is the probability of finding an atom of a particular type at height z, z_0 is the interface height, and w is the width of the interface. Every atom in the IrMn layer is initially set as Ir or Mn and then has a probability (P) of being changed to a Cu atom depending on its height (z). The reverse process is done for the mixing of Ir and Mn into the Cu layers. The width of the interface was systematically varied between 0 and 0.5 nm as shown schematically in Fig 3.

The temperature dependent sublattice magnetization and isotropic susceptibility were calculated for varying thicknesses of IrMn$_3$. Due to the large scatter in the calculated properties in the lowest film thicknesses, the simulations are averaged over 10 different sample crystal structures with different pseudorandom number sequences in the Monte Carlo algorithm to obtain average data for the mean sublattice magnetization and susceptibility. A typical set of data for thickness $t_{IrMn} = 1$ nm and atomically flat interface $w = 0$ nm is shown in Fig. 4 comparing the (a) disordered γ and (b) L1$_2$ phases. The simulations show a significant decrease in the Néel temperature for both phases due to the missing interface Mn-Mn exchange bonds. In particular, the γ phase shows a Néel temperature close to room temperature even for an atomically smooth interface, suggesting that films thinner than this are unsuitable for applications in spintronics.

Interestingly, the zero temperature ordering of the disordered γ phase obtained from the field cooling simulation is
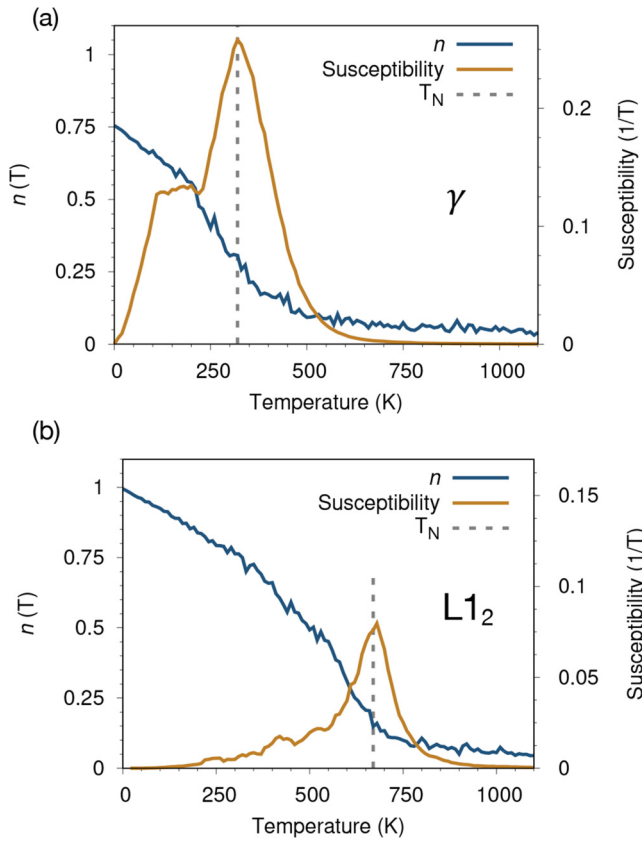
FIG. 4. Simulated temperature dependent sublattice magnetization curves and isotropic susceptibility for a 1 nm thick thin film of $IrMn_3$ comparing γ (a) and $L1_2$ (b) phases for a system with a perfectly flat interface. The data are averaged over ten statistically independent samples. The points show simulated data and the line is a fit using Eq. (2). Both curves show a significant reduction in the Néel temperature compared to bulk and reduced criticality near T_N due to the small finite thickness of the film.

significantly less than 1, with a global ordering fraction around 0.7. The small size of the system means that the spins should form a single antiferromagnetic domain. However, the random distribution of the Ir sites in the crystal means that some areas of the AFM are weakly coupled to the rest allowing a stable antiferromagnetic domain to form. This effect is unique to thin films, since in the bulk there is a path which allows the exchange coupling of regions around Ir-rich regions of low coupling, while in very thin films, the percolation route in one dimension is constrained and leads to decoupling of different regions of the crystal. This suggests that even in the absence of thermal fluctuations, full ordering of the $IrMn_3$ at nanoscale sizes may be difficult to achieve. A side effect of the intrinsically low magnetic order is a discontinuity in the isotropic susceptibility at very low temperatures. Here, infinitesimal thermal fluctuations of the spins lead to a large variation of the sublattice magnetization, in strong contrast to the fully ordered $L1_2$ phase which has a low susceptibility at low temperatures. This is an unusual effect and may be measurable as an intrinsic instability of the antiferromagnetic spin structure.

A systematic study of the effect of film thickness and intermixing on the Néel temperature is shown in Fig. 5 for the γ (a) and $L1_2$ (b) phases alongside comparative simulation data for a generic FCC ferromagnet with a Curie temperature

the same as the Néel temperature. Both antiferromagnetic phases show a stronger finite size effect than the comparable ferromagnetic film, with a stronger reduction in the ordering (Néel) temperature for a given film thickness. This is likely due to the geometric spin frustration which increases the influence of the thermal spin fluctuations on the sublattice ordering. Comparing the two phases of $IrMn_3$, the γ phase shows a stronger finite size effect and larger reduction in the Néel temperature compared to the ordered phase. We attribute this to the reduction in global sublattice magnetic order in the γ phase due to the formation of antiferromagnetic domains and larger effect of thermal fluctuations. For the thinnest films, there is a catastrophic reduction of the Néel temperature to a few degrees Kelvin which is not seen in the ferromagnetic case. Here, we believe that the origin is due to the percolation effect where locally antiferromagnetic order
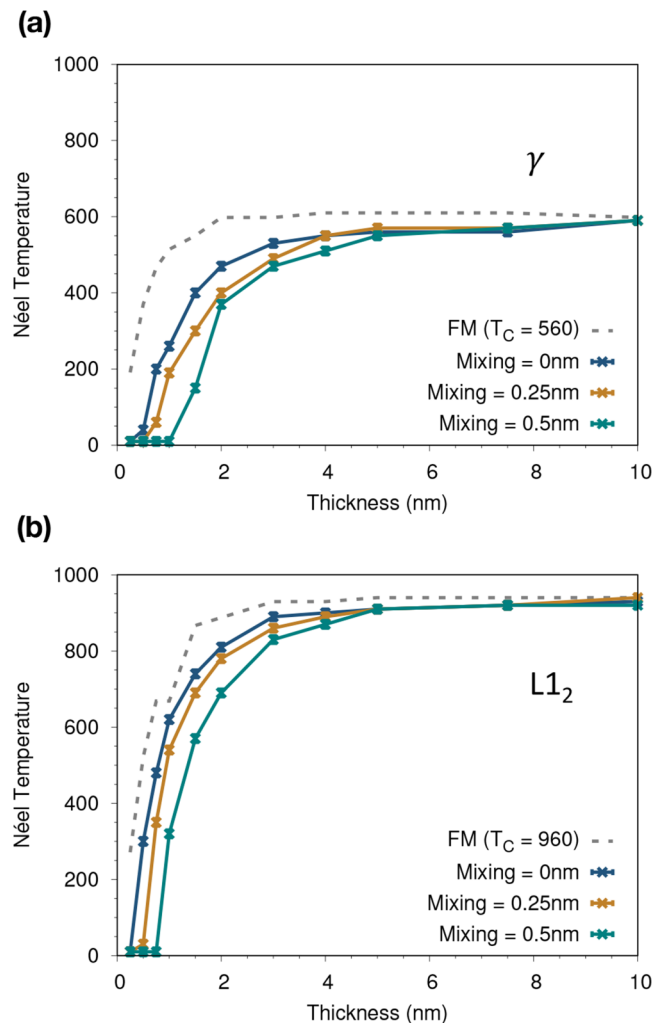

FIG. 5. Simulated systematic variation in the Néel temperature with varying film thickness for IrMn in both the γ (a) and $L1_2$ phases (b) for different interfacial mixing widths. The dashed lines show comparative data for a ferromagnet with the Curie temperature $T_C = T_N$ for each phase. The data show a systematic decrease in the Néel temperature for thinner films and a stronger finite size effect in the γ phase compared to the $L1_2$ phase. In both cases, the finite size variation of the Néel temperature shows a stronger decrease than the equivalent ferromagnet (FM) due to the inherent spin disorder. Intermixing of the IrMn with a non-magnetic Cu layer shows an enhanced finite size effect for increased mixing due to a larger number of missing exchange bonds.

still exists, but even on the nanoscale, the long range order is disrupted leading to an apparent low Néel temperature over the total simulated sample. These effects may be more severe for laterally larger films which would typically be used in devices.

Finally, we consider the effect of intermixing to emulate the effect of sputtered thin films as shown by the comparative data in Fig. 5. It is clear from the data that larger interfacial mixing leads to a larger reduction of the Néel temperature of the films compared to the atomically smooth interface. The effect also seems to be larger for the γ phase compared to the ordered $L1_2$ phase, likely due to the random intermixing increasing the exchange decoupling of different regions of the antiferromagnet and reducing the global ordering. For the thicker films $t_{IrMn} > 3$ nm, the effects of intermixing on the Néel temperature is much weaker and likely negligible for devices operating close to room temperature.

V. DISCUSSION

We have investigated the effect of film thickness and intermixing on the temperature dependent properties of antiferromagnetic $IrMn_3$ alloys using an atomistic spin model and Monte Carlo Metropolis simulations. The temperature dependent magnetic properties of the ordered $L1_2$ and disordered γ phases of $IrMn_3$ have been calculated for ultra thin films from which we extract the sublattice susceptibility and Néel ordering temperature. We find a relatively strong finite size effect compared to a ferromagnetic system arising due to spin frustration and a larger influence of thermal spin fluctuations on the magnetic order. For the thinnest γ-$IrMn_3$ films, we find a collapse of the Néel temperature to less than room temperature making them unsuitable for devices due to their large thermal spin fluctuations and instability. In general, moderate intermixing has a weak effect for films thicker than 3 nm, but causes a severe reduction in the Néel temperature for the thinnest films. We conclude that more control of the film properties and the use of thicker layers is required for devices utilizing antiferromagnetic IrMn films compared to equivalent ferromagnetic thin films. Although the results from our study are specific to $IrMn_3$, we expect that other antiferromagnets with a similarly complex spin structure will also show strong finite size effects, for example, PtMn and FeMn. Simple two-sublattice antiferromagnets such as CoO, NiO, CuMnAs, and Mn_2Au conversely have a lower degree of spin frustration and so may not be as susceptible to finite size effects and therefore may be better suited to applications.

ACKNOWLEDGMENTS

[1]T. Jungwirth, J. Sinova, A. Manchon, X. Marti, J. Wunderlich, and C. Felser, "The multiple directions of antiferromagnetic spintronics," Nat. Phys. **14**(3), 200–203 (2018).

[2]V. Baltz, A. Manchon, M. Tsoi, T. Moriyama, T. Ono, and Y. Tserkovnyak, "Antiferromagnetic spintronics," Rev. Mod. Phys. **90**, 015005 (2018).

[3]L. Néel, "Magnetism and local molecular field," Science **174**(4013), 985–992 (1971).

[4]D. Apalkov, B. Dieny, and J. M. Slaughter, "Magnetoresistive random access memory," Proc. IEEE **104**(10), 1796–1830 (2016).

[5]I. L. Prejbeanu, M. Kerekes, R. C. Sousa, H. Sibuet, O. Redon, B. Dieny, and J. P. Nozi'eres, "Thermally assisted MRAM," J. Phys. Condens. Matter **19**(16), 165218 (2007).

[6]P. Wadley, B. Howells, J. Železný, C. Andrews, V. Hills, R. P. Campion, V. Novák, K. Olejník, F. Maccherozzi, S. S. Dhesi, S. Y. Martin, T. Wagner, J. Wunderlich, F. Freimuth, Y. Mokrousov, J. Kuneš, J. S. Chauhan, M. J. Grzybowski, A. W. Rushforth, K. W. Edmonds, B. L. Gallagher, and T. Jungwirth, "Electrical switching of an antiferromagnet," Science **351**(6273), 587–590 (2016).

[7]M. Meinert, D. Graulich, and T. Matalla-Wagner, "Electrical switching of antiferromagnetic Mn_2Au and the role of thermal activation," Phys. Rev. Appl. **9**, 064040 (2018).

[8]D. Ielmini, "Brain-inspired computing with resistive switching memory (RRAM): Devices, synapses and neural networks," Microelectron. Eng. **190**, 44–53 (2018).

[9]M. Sharad, D. Fan, and K. Roy, "Spin-neurons: A possible path to energy-efficient neuromorphic computers," J. Appl. Phys. **114**(23), 234906 (2013).

[10]S. Fukami, C. Zhang, S. DuttaGupta, A. Kurenkov, and H. Ohno, "Magnetization switching by spin–orbit torque in an antiferromagnet–ferromagnet bilayer system," Nat. Mater. **15**, 535 (2016).

[11]W. A. Borders, H. Akima, S. Fukami, S. Moriya, S. Kurihara, Y. Horio, S. Sato, and H. Ohno, "Analogue spin-orbit torque device for artificial-neural-network-based associative memory operation," Appl. Phys. Express **10**(1), 013007 (2017).

[12]L. Frangou, S. Oyarzún, S. Auffret, L. Vila, S. Gambarelli, and V. Baltz, "Enhanced spin pumping efficiency in antiferromagnetic IrMn thin films around the magnetic phase transition," Phys. Rev. Lett. **116**, 077203 (2016).

[13]A. Kohn, A. Kovács, R. Fan, G. J. McIntyre, R. C. C. Ward, and J. P. Goff, "The antiferromagnetic structures of IrMn3 and their influence on exchange-bias," Sci. Rep. **3**, 2412 (2013).

[14]I. Tomeno, H. N. Fuke, H. Iwasaki, M. Sahashi, and Y. Tsunoda, "Magnetic neutron scattering study of ordered Mn3Ir," J. Appl. Phys. **86**, 3853–3856 (1999).

[15]L. Szunyogh, L. Udvardi, J. Jackson, U. Nowak, and R. Chantrell, "Atomistic spin model based on a spin-cluster expansion technique: Application to the $IrMn_3$/Co interface," Phys. Rev. B **83**, 024401 (2011).

[16]L. Szunyogh, B. Lazarovits, L. Udvardi, J. Jackson, and U. Nowak, "Giant magnetic anisotropy of the bulk antiferromagnets irmn and $IrMn_3$ from first principles," Phys. Rev. B **79**, 020403 (2009).

[17]D. Petti, E. Albisetti, H. Reichlová, J. Gazquez, M. Varela, M. Molina-Ruiz, A. F. Lopeandía, K. Olejník, V. Novák, I. Fina, B. Dkhil, J. Hayakawa, X. Marti, J. Wunderlich, T. Jungwirth, and R. Bertacco, "Storing magnetic information in IrMn/Mgo/Ta tunnel junctions via field-cooling," Appl. Phys. Lett. **102**(19), 192404 (2013).

[18]R. F. L. Evans, W. J. Fan, P. Chureemart, T. A. Ostler, M. O. A. Ellis, and R. W. Chantrell, "Atomistic spin model simulations of magnetic nanomaterials," J. Phys. Condens. Matter **26**(10), 103202 (2014). s

[19]L. Néel, "Anisotropie magnétique superficielle et surstructures d'orientation," J. Phys. Radium **15**(4), 225–239 (1954).

[20]D. Hinzke, and U. Nowak, "Monte Carlo simulation of magnetization switching in a Heisenberg model for small ferromagnetic particles," Comput. Phys. Commun. **121–122**, 334–337 (1999). Proceedings of the Europhysics Conference on Computational Physics CCP 1998.

[21]VAMPIRE software package, version 5, 2017 , see http://vampire.york.ac.uk.